RNA-silencing induces target gene relocalization toward a specialized nuage domain

Yuchen Yang[1,] , David Grunwald[1,] , James R. Priess[,2,3] and Craig C. Mello[1,4,5*]

Author Affiliations:

1. RNA Therapeutics Institute, University of Massachusetts Medical School, Worcester, MA 01605
2. Fred Hutchinson Cancer Research Center, Seattle, Washington, United States
3. Department of Biology, University of Washington, Seattle, Washington, United States
4. Program in Molecular Medicine, University of Massachusetts Medical School, 368 Plantation Street, Worcester, MA, 01605 United States
5. Howard Hughes Medical Institute, University of Massachusetts Medical School, Worcester, MA, USA

* Correspondence, Craig.Mello@umassmed.edu.

Abstract

Argonaute small RNA pathways maintain genome integrity and fertility by enforcing the transgenerational silencing of transposons as well as many developmentally regulated germline genes. To propagate silencing, Argonaute pathways coordinate heterochromatin silencing with cycles of small RNA amplification. In animal germlines, mRNA surveillance is thought to occur within cytoplasmic perinuclear domains called nuage. In *C. elegans,* nuage granules called P granules surround each pachytene germline nucleus. P granules are known to host many of the Argonaute small RNA systems that carry out transcriptome surveillance, but what if any specific roles P granules might play in Argonaute silencing have remained mysterious. Here we show that RNAi triggers the enlargement of a single P granule, which uniquely accumulates target RNA. P granule enlargement occurs independently of, and precedes transcriptional silencing, which culminates in the relocalization of both alleles of the target gene to the inner nuclear membrane (INM) directly adjacent the specialized P granule. Similarly, we show that piRNA-mediated silencing, causes both alleles of a targeted gene to reside near the INM adjacent to a P granule that uniquely contains target RNA sequences. Our findings suggest that nuage and its associated Argonaute pathways re-organize the three dimensional location of their genomic targets to facilitate RNA-guided inheritance.

Introduction

In the *C. elegans* germline, two major Argonaute pathways initiated by different mechanisms—the piRNA pathway(Watanabe and Lin, 2014) mediated by the Piwi Argonuate PRG-1 and the dsRNA-initiated RNAi pathway (Fire et al., 1998) mediated by the Argonaute RDE-1 (Chen et al., 2005)—rely on a common set of conserved downstream small RNA and chromatin effectors that maintain heritable silencing (Billi et al., 2014; Holoch and Moazed, 2015; Weiser and Kim, 2019). Argonaute proteins and the machinery that produces their small RNA cofactors localize to P granules (Updike and Strome, 2010), where they are thought to act in mRNA surveillance and in the amplification of small-RNA silencing signals (Billi et al., 2014; Weiser and Kim, 2019). In the *C. elegans* meiotic germline, each P granule is localized over a cluster of nuclear pores (Pitt et al., 2000), where it has the potential to intercept nascent mRNA *en route* to the cytoplasm (Sheth et al., 2010). Although previous cytological studies demonstrated the rapid loss of target mRNA in the cytoplasm during RNAi (Fire et al., 1998; Sheth et al., 2010), changes in the P granules or associated RNAs during silencing were not reported and the localization of target DNA was not examined. Thus, the dynamics and spatial relationships between nuage and the mRNA and DNA targets of silencing have remained mysterious.

Recent advances in RNA and DNA FISH technology have greatly enhanced the ability to track molecules at single-molecule resolution (Beliveau et al., 2015; Fields et al., 2019; Ji and van Oudenaarden, 2012). For example, splinted fluorescent probes that assemble multiple fluorophores at a single target greatly amplify DNA FISH signals and permit detection of single genes(Beliveau et al., 2015; Fields et al., 2019). Here we utilize

63 these improved reagents to revisit the cytological events associated with Argonaute
64 silencing.

65

66 **Results and Discussion**

67 To visualize the spatial and temporal response to RNAi, we exposed worms to dsRNA
68 targeting an abundantly transcribed germline-expressed gene, *oma-1*, and monitored
69 *oma-1* RNA- and DNA-FISH signals simultaneously over a time course of silencing. To
70 distinguish cytoplasmic and nuclear signals in RNA + DNA FISH experiments, we marked
71 the outer membrane of the nuclear envelope with a GFP::ZYG-12 fusion protein (Malone
72 et al., 2003) (Figure 1A-1F), while P granules were identified with GFP::GLH-1 (Figure
73 1G-1L) tagged at the endogenous *glh-1* locus by CRISPR genome editing (Ghanta et al.,
74 2020). We examined the pachytene region of the gonad, where germ cells are connected
75 to a large, shared region of cytoplasm called the core. As expected from previous studies,
76 oma-1 mRNA in untreated animals was present at low levels in many P granules, and
77 was abundant in the germ cell cytoplasm and gonad core (Figure 1J). A double dot of
78 *oma-1* RNA signal was visible inside each germ nucleus throughout the pachytene region
79 (Figure 1A, 1D and 1J). The nuclear RNA dots co-localized with *oma-1* DNA in
80 simultaneous RNA/DNA FISH experiments (Figure 1A), suggesting that they represent
81 transcription from the *oma-1* genes on the paired, homologous chromosomes.

82 As expected, RNAi induced a rapid, marked depletion of cytoplasmic *oma-1* mRNA
83 (for example, compare Figure 1A to 1B). In the same gonads, however, an *oma-1* RNA
84 signal appeared to increase within a single large, perinuclear focus adjacent to each

nucleus (Figure 1B and 1E). This perinuclear RNA signal was also present at 21 hours but was decreased in size (Figure 1C and 1F).

Prior to RNAi, the P granules varied in size (green signal in Figures 1G and 1J). However, after 6 hours of RNAi, one P granule on each nucleus appeared much larger than neighboring nuage (Figure 1H), and colocalized with the prominent, enlarged *oma-1* RNA focus (Figure 1K). Thus, RNAi appears to trigger differentiation between the P granules on the same nucleus, with target RNA accumulating in only one enlarged P granule. These results suggest that a single P granule becomes specialized for *oma-1* silencing.

The location of the *oma-1* RNA and DNA FISH signals within the nucleus exhibited dramatic changes during RNAi. Whereas prior to RNAi each pachytene nucleus exhibited two paired foci of DNA and the coincident RNA (Figure 1A), by 21 hours nuclei exhibited only a single focus of *oma-1* DNA and a coincident RNA signal (Figure 1C). These coincident signals were located near the INM (Figure 1F) and directly adjacent to the specialized P granule which, although now reduced in size, remained the only P granule that contained *oma-1* RNA (Figure 1I and 1L). The transition to a single focus of *oma-1* DNA and coincident RNA was evident in many nuclei by 6 hrs of *oma-1(RNAi)* (Figure 1B, inset ii), and when present this singular focus was always positioned near the INM adjacent the specialized P granule (Figure 1K, insets i and ii). Taken together these results suggest that RNAi causes the formation of a unique enlarged P granule where target RNA accumulates, and that formation of this specialized P granule precedes and possibly coordinates movement of the target DNA to the directly adjacent INM.

107 In order to determine whether genes in the RNAi pathway are required for the
108 specialized P granule, we repeated the above assays in the mutant *rde-3*. RDE-3 is an
109 effector of RNAi silencing that is required both in the animals exposed to dsRNA and for
110 inherited silencing among their offspring (Chen et al., 2005). As expected, in *rde-3*
111 mutants *oma-1* dsRNA did not trigger any of the cytological changes observed in wild-
112 type worms (compare Figures 2A and 2B with Figures 2C and 2D, respectively). For
113 example, the double dots of *oma-1* DNA did not relocalize toward the INM, low levels of
114 *oma-1* RNA remained visible in many P granules, which appeared similar in size to those
115 in untreated controls, and cytoplasmic *oma-1* mRNA remained abundant in the gonad
116 core (Figure 2A and 2B and Supplemental Figure 2).

117 Nuclear effectors of RNAi are known to drive heterochromatin formation and
118 several studies have linked heterochromatin formation to the localization of a silent gene
119 near the INM (Reviewed in (Ahringer and Gasser, 2018)). We therefore wondered
120 whether the nuclear effectors of the RNAi pathway are required for relocalization of the
121 target genes, and whether targeting events at nuclear transcription sites might precede
122 and drive P granule specialization. To explore these possibilities we examined the role of
123 two genes, the nuclear WAGO Argonaute, *wago-9/hrde-1* and its downstream effector
124 *nrde-2.* These genes are both required for establishment of heterochromatin at the target
125 locus and for transgenerational inheritance of silencing induced by RNAi (Ashe et al.,
126 2012; Buckley et al., 2012; Burton et al., 2011; Guang et al., 2010; Shirayama et al., 2012).
127 Importantly, neither gene is essential for RNAi when a dsRNA trigger is present, but rather
128 are only required for transmission of silencing to unexposed offspring. dsRNA triggered
129 the loss of cytoplasmic *oma-1* mRNA in both mutants, simlar to wild type, and the

130 accumulation of *oma-1* RNA in a single, enlarged P granule (Compare Figures 2E and
131 2G with Figure 2C). However, the nuclei retained two separate foci of DNA and coincident
132 RNA that did not relocalize toward the INM even after 21 hours of RNAi (compare Figure
133 2F and 2H to Figure 2D). Moreover, by 21 hrs, the unique enlarged P granule had
134 disappeared and *oma-1* RNA was detected in multiple smaller P granules (Fig 2F and
135 2H). Thus the nuclear events of RNAi are not required for the initial formation of the
136 specialized P granule, but instead function to promote its maintenance and to coordinate
137 the nuclear relocalization of the target genes into its proximity.

138 The *C. elegans* germline expresses tens of thousands of piRNAs that engage Piwi
139 Argonautes to direct transgenerational silencing of transposons and many protein-coding
140 genes (Billi et al., 2014). We wondered if piRNA silencing might also direct the
141 coordination of the target loci and a specialized P granule. To address this possibility we
142 examined the dosage compensation gene *xol-1*, which is a natural target of piRNA
143 silencing (Tang et al., 2018). Mutations in the Piwi Argonaute, *prg-1,* cause *xol-1*
144 expression in the germline and lead to dosage-compensation defects among progeny.
145 We first examined *prg-1* mutants to determine where *xol-1* is expressed when de-
146 repressed. Although *xol-1* was expressed at lower levels than oma-*1,* we found that late
147 pachytene nuclei in *prg-1* mutants had a pattern of *xol-1* DNA and RNA signals similar to
148 the pattern seen for *oma-1* in wild-type animals prior to dsRNA exposure. For example,
149 the nuclei each contained two foci of *xol-1* DNA and coincident RNA, and *xol-1* mRNA
150 was visible in several perinuclear P granules (Figures 3A and 3B). In contrast, late
151 pachytene germ cells in wild-type animals, where *xol-1* is repressed, exhibited a pattern
152 of *xol-1* DNA and RNA FISH signals similar to that of silenced *oma-1* after 21 hours of

153 RNAi (Figure 3C and 3D). For example, the *xol-1* genes appeared as a single dot
154 coincident with the *xol-1* nuclear RNA signal, and were localized adjacent to a P granule
155 enriched for *xol-1* RNA. Thus, the cytology of the PRG-1-dependent OFF state of *xol-1* in
156 wild-type animals resembles the dsRNA-induced OFF state of a gene targeted by RNAi.

157 We wondered whether different P granules become specialized to silence distinct
158 targets. To address this possibility we decided to monitor both *oma-1* and *xol-1*
159 simultaneously in wild-type animals over a time course of *oma-1(RNAi).* The *oma-1* and
160 *xol-1* genes are on different chromosomes, and their respective nuclear signals of DNA
161 and RNA generally remained well separated over the time course of RNAi (Figure 3E and
162 3F). For example at 6 hr of RNAi the enlarged, specialized P granule associated with
163 *oma-1* silencing formed independently of the nuclear transcription site of *xol-1* and its
164 associated P granule (Figure 3E), and at 21 hr of RNAi the *oma-1* genes were positioned
165 near the INM independently of the *xol-1* DNA (Figure 3F). Together these findings
166 suggest that each P granule promotes silencing of distinct genomic targets, and that the
167 three dimensional positioning of the genome is stochastic at least with regard to the
168 ultimate disposition of the silenced *oma-1* and *xol-1* genes at the INM.

169 In summary, we have shown that RNAi- and piRNA-mediated silencing trigger the
170 specialization of a P granule. Nuclear silencing components direct the re-localization of
171 the target genes into proximity of this specialized P granule but are not required for its
172 formation. Each domain of nuage appears to serve distinct RNA targets which become
173 spatially linked to their corresponding genomic DNA targets. After the target genes
174 relocate, the nuage diminishes in size, perhaps reflecting the reduced transcriptional
175 activity of the target locus. Thus our results suggest that the transcriptional silencing

176 machinery participates in a feedback loop that redirects the target loci and mRNA export
177 to a single specialized P granule. The continued low-level transcription of the paired loci
178 at the INM may serve to supply the adjacent specialized nuage with template RNA that
179 feeds small RNA amplification and inherited silencing.

180 Thousands of *C. elegans* germline mRNAs are targeted by nearly one million
181 distinct Argonaute guide complexes. How the system can simultaneously utilize this
182 multitude of Argonautes to surveil gene expression has been entirely mysterious. Our
183 findings suggest a partial answer to this mystery. Approximately 20 to 50 P granules
184 surround each pachytene nucleus. Therefore, if each P granule is specialized to handle
185 a subset of the RNA silencing load, each P granule need only harbor 50- to 20-thousand
186 guide complexes, instead of nearly one million. Moreover by directing the co-localization
187 of their target genes each P granule need service only 30 to 75 of the approximately 1500
188 protein coding genes that are targeted by the system transgenerationally (Gu et al., 2009).

189 Our findings suggest that each P granule is initially seeded with, or differentiates
190 to contain, distinct RNA information and that P granules utilize this information to guide
191 the transgenerational regulation of their target genes. During late oogenesis, some P
192 granules dissociate from germ nuclei; the dissociated P granules mix in the shared core
193 cytoplasm, and are taken up by enlarging oogonia (Wolke et al., 2007). P granules have
194 liquid-like properties (Brangwynne et al., 2009) and in early embryos maternally-derived
195 P granules appear to dissolve and reform in germline blastomeres (Seydoux, 2018).
196 These embryonic P granules co-localize with parentally derived Argonaute guide
197 complexes (Claycomb et al., 2009; Gu et al., 2009). Mutations that disrupt embryonic P
198 granules impair transgenerational inheritance of Argonaute silencing signals (Dodson

199 and Kennedy, 2019; Ouyang et al., 2019). Thus it seems likely that when gene expression
200 initiates in embryonic germ cell progenitors, inherited silencing signals in these embryonic
201 P granules guide the relocalization of germline chromatin to initiate a new round of guide
202 RNA biogenesis, nuage differentiation, and chromatin re-localization.

203 We do not know how P granules compartmentalize and transmit information across
204 generations. For example, do Argonaute-guide complexes that assemble in each
205 pachytene P granule, remain together, or do they become shuffled during the dynamics
206 of early embryogenesis? Similarly, the questions of how nuage becomes specialized and
207 how it orchestrates DNA relocalization will require further study. The image of nuage that
208 emerges from these studies mirrors Darwin's notion of gemmules as the units of heredity
209 (Choi and Mango, 2014; Liu, 2018)—seeds of parental information that accumulate in
210 germ cells to guide inheritance.

211 **Acknowledgements:** We thank Susan Strome from UC Santa Cruz, and Karen Bennett
212 from University of Missouri School of Medicine for kindly gifting reagents, Christina Baer
213 from SCOPE at UMMS for support with the micromanager installation. We thank Darryl
214 Conte, and members of the Mello and Grunwald labs for help with preparation of the
215 manuscript. This work was supported by a Howard Hughes Medical Institute
216 Investigatorship and NIH R37GM058800 (C.C.M), NSF grant 1614940 (D.G.), and NIH
217 RO1GM098583 (J.R.P). . Some of the strains used in this work were provided by the
218 Caenorhabditis Genetic Center, which is funded by the NIH National Center for Research
219 Resources (NCRR).

220

221

222

223 **Methods:**

224 **Worm culture and strains:**

225 The wild-type strain N2 was used and nematodes were cultured as described(Brenner,
226 1974). The following transgenic strains were used: **JJ2101**: *zuIs242;* [*nmy-2p*::*pgl-1*::*gfp*
227 + *unc-119(+)*] (Sheth et al., 2010), **WH223**: *ojIs*9; [*zyg-12*::*gfp* + *unc-119(+)*], **JJ2212**:
228 [*nmy-2p*::*pgl-1*::*mrfp*]. and **WM455**, *gfp::flag::xol-1*(*ne4555*) (Tang et al., 2018). **WM704**
229 *glh-1(ne4816[gfp::glh-1])* was generated by CRISPR genome editing as described in
230 (Ghanta et al., 2020).

231

232 **Sample preparation for combined FISH, GFP detection and Immunofluorescence**

233 General techniques for gonad dissections were used as described (Raiders et al., 2018).
234 Briefly, worms were rinsed free of bacteria, then collected in PBS containing 0.1 mM
235 tetramisole (SIGMA L9756) as a paralytic. Once the worms stopped moving, they were
236 placed in PBS for dissection. In some preparations, 0.1% Tween-20 was used to facilitate
237 gonad transfer by micropipette. The dissected gonads were suspended briefly in buffer A
238 (75 mM Hepes (pH 6.9), 40 mM NaCL, 5 mM KCL, 2 mM MgCL2, 1 mM EGTA; all
239 chemicals from Sigma), to which was added a equal volume of fixative buffer B (5%
240 paraformaldehyde, 7.5 mM Hepes (pH 7.2), 12 mM NaCL, 1.0 mM KCL, 0.6 mM MgCL2,
241 0.3 mM EGTA; all chemicals from Sigma). After fixing for 15 mins, the gonads were rinsed,
242 then incubated in RNase-free PBS (ThermoFisher AM9624) containing 0.1% Triton-X100
243 (Sigma) for 10 mins. The gonads were transferred to room temperature MeOH for 10

244 mins, then placed in fixative buffer B for an additional 5 mins and rinsed in PBS. Gonads
245 were then dehydrated and stored in EtOH.

246 **RNA and DNA FISH**

247 Gonads stored in EtOH were rehydrated in an EtOH/PBS series (10%, 20%, 60% EtOH),
248 then rinsed and incubated in two changes of wash buffer C (10% formamide, 2XSSC
249 [0.3M NaCL, 30 mM sodium citrate (7.0)], each rehydration and rinse step was 5 minutes.
250 Then the sample was incubated with three changes of wash buffer C as follows: 60°C for
251 1-3 min, 70°C for 3 min, followed by 60°C for 10-20 min.

252 The wash buffer was replaced with a solution containing ~0.01μM oligo probes
253 (RNA and primary DNA probes), 90% RNA FISH hybridization buffer (Stellaris SMF-HB-
254 1), and 10% deionized formamide, and incubated at 37ºC overnight in the dark. The
255 samples were rinsed and incubated in wash buffer C for 10 mins at room temperature,
256 then incubated in fresh wash buffer at 37ºC for 1 hr. The wash buffer was removed and
257 replaced with fresh wash buffer C at 37ºC for 1 hr. Gonads were rinsed and kept in PBS
258 for immunostaining experiments.

259 For combined RNA and DNA FISH experiments, the gonads were treated with an
260 additional solution containing 0.01 μM Bridge oligo, 0.01μM detection oligo in 2XSSC, 30%
261 formamide at room temperature for 3 hrs. Gonads were washed in prewarmed 2XSSC at
262 60ºC for 20 min, followed by two washes in 2XSSCT (2XSSC with 0.3% Triton X-100) at
263 60ºC for 5 min each, and a wash in 2XSSCT at 60ºC for 20 min. Samples were then
264 rinsed at room temperature in 2XSSC, then rinsed and kept in PBS.

265 **Immunostaining**

266 After the FISH protocol was complete gonads in PBS were incubated with primary
267 antibodies diluted in PBS and 0.5 units/µl of RNasin (Promega N261A) at 4ºC overnight.
268 The antibody solution was removed and the slides rinsed in three changes of PBS, 5 min
269 each. The gonads were then incubated in secondary antibodies diluted in PBS and 0.5
270 units/µl of RNasin at room temperature for 2 hours. The gonads were rinsed briefly in
271 PBS, then immersed in mounting medium with DAPI (Vectashield H-2000) for imaging.
272 The following antibodies were used: Rabbit anti-PGL-1, a gift from Susan Strome,
273 (Kawasaki et al., 1998) Chicken anti-GLH-2, a gift from Karen Bennett (Gruidl et al., 1996).
274

275 **Microscope settings and configuration:**

276 All images were acquired on a Yokogawa CSU21 spinning disk confocal microscope
277 mounted onto an Axiovert 200M and operated with Micromanager(Edelstein et al., 2010)
278 software. The sample was mounted using a slide holder and motorized stage (ASI), and
279 images were acquired with a Zeiss 63x (1.4 NA) Planapo oil immersion objective. Optical
280 z stacks were collected at increments of 0.5 microns. The spinning disk unit added roughly
281 a 2.5 x magnification factor resulting in a pixel size of ~100 nm in the image plane. Images
282 were acquired with a Hamamatsu ImageEM (model C9100-13) series camera using an
283 EM gain of 300 and set to free read mode. Light from four lasers in a custom laser module
284 (made by Solamere) containing 405 nm, 488 nm, 561 nm and 640 nm laser lines was
285 coupled into a monomode optical fiber and delivered to the Yokogawa scan head. The
286 following bandpass filters (Chroma) were used as emission filters ET-460-50, ET-525-50,
287 ET-605-52, ET-700-75. Laser power was adjusted for each sample to minimize sample
288 bleaching. Typical acquisition times were between 400-500 msecs/frame.

Image processing:

Composite images were stitched from 9 sub-images that have 50% overlapping with adjacent images (Preibisch et al., 2009), but subregions were cropped to size to show desired features in the final figure. Spatial offsets between color channels in lateral (x,y) and axial (z) directions were estimated using 500 nm sized four color-stained beads (Tetraspecks, Thermo Fisher, Catalog number T14792). The center plane is defined as the plane with the largest diameter signal within a bead and was determined manually in an unprocessed image stack. Raw image stacks, after axial offset correction, were filtered using a Gaussian kernel with a width σ = 1, a Laplacian of Gaussian (LoG3D filter (Sage et al., 2005)) followed by a Gaussian kernel with a width σ = 1. LoG3D is used for background suppression and not to localize the exact position of a spot. The sigma along the optical axis is taken as roughly half the number of slices the signal is visible in. This approach preserves the visual impression of signal dimension between the channels. The sigma for each channel used was: Ch1: $\sigma_{x,y}$ = 1 pixel, σ_z = 2 pixel; Ch2: $\sigma_{x,y}$ = 1pixel, σ_z = 2 pixel; Ch3: $\sigma_{x,y}$ = 1 pixel, σ_z = 2 pixel.

306

307 **Figure legends:**

308 **Figure 1.** Pachytene germ nuclei in adult hermaphrodite gonads examined at 0, 6, and
309 21 hours after exposure to *oma-1* dsRNA [*oma-1(RNAi)*]. Single gonads are shown in the
310 paired panels A/D, B/E, C/F, G/J, H/K, and I/L. The larger image in each panel shows an
311 optical z-projection of about 30 planes, corresponding to approximately half the thickness
312 of the gonad. The three smaller insets show high magnifications of single optical planes
313 through individual nuclei**.** (A-L) Confocal images of RNA FISH, DNA FISH, and
314 fluorescent-protein signals (P granule = GFP:GLH-1 and Nuclear Env =ZYG-12::GFP).
315 Signals were colored either green or magenta as indicated at top, such that coincident
316 signals appear white. For example, perinuclear RNA in panel D is magenta, but the
317 nuclear RNA appears white because it is coincident with the green DNA signal. Before,
318 and at early timepoints in, *oma-1(RNAi)*, the pair of nuclear foci of DNA and coincident
319 appear within a small radius around the synapsed, pachytene chromosomes, and appear
320 randomly oriented with respect to the nuclear envelope (panels A and B). By 21 hrs, a
321 single focus of DNA and coincident RNA appears juxtaposed to the envelope (panel C).
322 Prior to RNAi most cytoplasmic *oma-1* mRNA in the gonad is contained in the shared
323 core region underlying the nuclei and appears as a central, vertical band in panels A, D,
324 and J.

325

326 **Figure 2.** Wild-type or mutant gonads exposed to *oma-1* dsRNA for 6hr or 21 hrs as
327 indicated. Images are confocal images, as in Figure 1 with signals represented in green

328 or magenta, and merged, coincident signals in white. P granules were detected using a
329 antiserum specific for GLH-2.

330

331 **Supplemental Figure 2**. Wild-type or mutant gonads as indicated exposed to *oma-1*
332 dsRNA for 0hr. Images are confocal images, as in Figure 1 and 2.

333

334 **Figure 3.** (A-F) Merged confocal images as in Figures 1 and 2 of dissected gonads
335 isolated from strains that encode gfp fused to the endogenous *xol-1* gene. DNA and RNA
336 FISH signals were detected with both *xol-1* and *gfp* specific probes (see Methods). (A-D)
337 Merged confocal images of the pachytene zones in wt (A B) and *prg-1* mutants (C D).
338 Insets show single Z sections of representative nuclei. (E and F) Simultaneous detection
339 of P granules and *oma-1* and *xol-1* RNA (E) or DNA (F) in late pachytene wildtype gonads
340 after exposure to *oma-1* dsRNA for 6 hours (E) or 21 hours (F). The *oma-1* and *xol-1*
341 signals were in different regions of the nucleus, and in general were not both visible in a
342 single focal plane, therefore the separation of these signals in individual nuclei is
343 illustrated here by a projection of optical z planes through the entire nuclei (paired
344 arrowheads in E and F). The colocalization of *xol-1* RNA and P granule signal in (E) was
345 barely visible in this composite where contrast was adjusted to detect the much more
346 intense *oma-1* RNA P granule signal. P granules were detected using a mixture of
347 antisera specific for GLH-2 and PGL-1.

348

349 **Figure 4.** Model illustrating events in RNA silencing. In the top panels the initiation of
350 silencing induces clearance of cytoplasmic mRNA by cytoplasmic WAGO Argonautes

351 (yellow Argonautes in the model). By 6 hours, the RNA signal becomes limited to a single
352 P granule which expands to support the amplification of small RNAs and to coordinate
353 the programming of nuclear Argonautes (blue). Nuclear silencing in turn initiates
354 heterochromatin formation and the capture of the target genes in proximity to the adjacent
355 INM. After the target genes spatially connect to nuage, the nuage diminishes in size.
356 When the nuclear RNAi machinery is disarmed by mutation (lower panel), a single
357 enlarged P granule still forms, but the target genes fail to relocalize to the nuclear
358 periphery, and mRNA once again accumulates in multiple P granules.

359

360 References:

361

362

363 Ahringer, J., and Gasser, S.M. (2018). Repressive Chromatin in Caenorhabditis elegans:
364 Establishment, Composition, and Function. Genetics *208*, 491-511.
365 Ashe, A., Sapetschnig, A., Weick, E.M., Mitchell, J., Bagijn, M.P., Cording, A.C., Doebley, A.L.,
366 Goldstein, L.D., Lehrbach, N.J., Le Pen, J.*, et al.* (2012). piRNAs can trigger a multigenerational
367 epigenetic memory in the germline of C. elegans. Cell *150*, 88-99.
368 Beliveau, B.J., Boettiger, A.N., Avendano, M.S., Jungmann, R., McCole, R.B., Joyce, E.F., Kim-
369 Kiselak, C., Bantignies, F., Fonseka, C.Y., Erceg, J.*, et al.* (2015). Single-molecule super-
370 resolution imaging of chromosomes and in situ haplotype visualization using Oligopaint
371 FISH probes. Nat Commun *6*, 7147.
372 Billi, A.C., Fischer, S.E., and Kim, J.K. (2014). Endogenous RNAi pathways in C. elegans.
373 WormBook, 1-49.
374 Brangwynne, C.P., Eckmann, C.R., Courson, D.S., Rybarska, A., Hoege, C., Gharakhani, J.,
375 Julicher, F., and Hyman, A.A. (2009). Germline P granules are liquid droplets that localize by
376 controlled dissolution/condensation. Science *324*, 1729-1732.
377 Brenner, S. (1974). The genetics of Caenorhabditis elegans. Genetics *77*, 71-94.
378 Buckley, B.A., Burkhart, K.B., Gu, S.G., Spracklin, G., Kershner, A., Fritz, H., Kimble, J., Fire, A.,
379 and Kennedy, S. (2012). A nuclear Argonaute promotes multigenerational epigenetic
380 inheritance and germline immortality. Nature *489*, 447-451.
381 Burton, N.O., Burkhart, K.B., and Kennedy, S. (2011). Nuclear RNAi maintains heritable gene
382 silencing in Caenorhabditis elegans. Proc Natl Acad Sci U S A *108*, 19683-19688.

383 Chen, C.C., Simard, M.J., Tabara, H., Brownell, D.R., McCollough, J.A., and Mello, C.C. (2005). A
384 member of the polymerase beta nucleotidyltransferase superfamily is required for RNA
385 interference in C. elegans. Curr Biol *15*, 378-383.
386 Choi, Y., and Mango, S.E. (2014). Hunting for Darwin's gemmules and Lamarck's fluid:
387 transgenerational signaling and histone methylation. Biochim Biophys Acta *1839*, 1440-
388 1453.
389 Claycomb, J.M., Batista, P.J., Pang, K.M., Gu, W., Vasale, J.J., van Wolfswinkel, J.C., Chaves, D.A.,
390 Shirayama, M., Mitani, S., Ketting, R.F.*, et al.* (2009). The Argonaute CSR-1 and its 22G-RNA
391 cofactors are required for holocentric chromosome segregation. Cell *139*, 123-134.
392 Dodson, A.E., and Kennedy, S. (2019). Germ Granules Coordinate RNA-Based Epigenetic
393 Inheritance Pathways. Dev Cell *50*, 704-715 e704.
394 Edelstein, A., Amodaj, N., Hoover, K., Vale, R., and Stuurman, N. (2010). Computer control of
395 microscopes using microManager. Curr Protoc Mol Biol *Chapter 14*, Unit14 20.
396 Fields, B.D., Nguyen, S.C., Nir, G., and Kennedy, S. (2019). A multiplexed DNA FISH strategy
397 for assessing genome architecture in Caenorhabditis elegans. Elife *8*.
398 Fire, A., Xu, S., Montgomery, M.K., Kostas, S.A., Driver, S.E., and Mello, C.C. (1998). Potent and
399 specific genetic interference by double-stranded RNA in Caenorhabditis elegans. Nature *391*,
400 806-811.
401 Gruidl, M.E., Smith, P.A., Kuznicki, K.A., McCrone, J.S., Kirchner, J., Roussell, D.L., Strome, S.,
402 and Bennett, K.L. (1996). Multiple potential germ-line helicases are components of the germ-
403 line-specific P granules of Caenorhabditis elegans. Proc Natl Acad Sci U S A *93*, 13837-13842.
404 Gu, W., Shirayama, M., Conte, D., Jr., Vasale, J., Batista, P.J., Claycomb, J.M., Moresco, J.J.,
405 Youngman, E.M., Keys, J., Stoltz, M.J.*, et al.* (2009). Distinct argonaute-mediated 22G-RNA
406 pathways direct genome surveillance in the C. elegans germline. Mol Cell *36*, 231-244.
407 Guang, S., Bochner, A.F., Burkhart, K.B., Burton, N., Pavelec, D.M., and Kennedy, S. (2010).
408 Small regulatory RNAs inhibit RNA polymerase II during the elongation phase of
409 transcription. Nature *465*, 1097-1101.
410 Holoch, D., and Moazed, D. (2015). RNA-mediated epigenetic regulation of gene expression.
411 Nat Rev Genet *16*, 71-84.
412 Ji, N., and van Oudenaarden, A. (2012). Single molecule fluorescent in situ hybridization
413 (smFISH) of C. elegans worms and embryos. WormBook, 1-16.
414 Kawasaki, I., Shim, Y.H., Kirchner, J., Kaminker, J., Wood, W.B., and Strome, S. (1998). PGL-1,
415 a predicted RNA-binding component of germ granules, is essential for fertility in C. elegans.
416 Cell *94*, 635-645.
417 Liu, Y. (2018). In Search of Darwin's Imaginary Gemmules. Adv Genet *101*, 87-114.
418 Malone, C.J., Misner, L., Le Bot, N., Tsai, M.C., Campbell, J.M., Ahringer, J., and White, J.G. (2003).
419 The C. elegans hook protein, ZYG-12, mediates the essential attachment between the
420 centrosome and nucleus. Cell *115*, 825-836.
421 Ouyang, J.P.T., Folkmann, A., Bernard, L., Lee, C.Y., Seroussi, U., Charlesworth, A.G., Claycomb,
422 J.M., and Seydoux, G. (2019). P Granules Protect RNA Interference Genes from Silencing by
423 piRNAs. Dev Cell *50*, 716-728 e716.
424 Pitt, J.N., Schisa, J.A., and Priess, J.R. (2000). P granules in the germ cells of Caenorhabditis
425 elegans adults are associated with clusters of nuclear pores and contain RNA. Dev Biol *219*,
426 315-333.
427 Preibisch, S., Saalfeld, S., and Tomancak, P. (2009). Globally optimal stitching of tiled 3D
428 microscopic image acquisitions. Bioinformatics *25*, 1463-1465.

429 Raiders, S.A., Eastwood, M.D., Bacher, M., and Priess, J.R. (2018). Binucleate germ cells in
430 Caenorhabditis elegans are removed by physiological apoptosis. PLoS Genet *14*, e1007417.
431 Sage, D., Neumann, F.R., Hediger, F., Gasser, S.M., and Unser, M. (2005). Automatic tracking of
432 individual fluorescence particles: application to the study of chromosome dynamics. IEEE
433 Trans Image Process *14*, 1372-1383.
434 Seydoux, G. (2018). The P Granules of C. elegans: A Genetic Model for the Study of RNA-
435 Protein Condensates. J Mol Biol *430*, 4702-4710.
436 Sheth, U., Pitt, J., Dennis, S., and Priess, J.R. (2010). Perinuclear P granules are the principal
437 sites of mRNA export in adult C. elegans germ cells. Development *137*, 1305-1314.
438 Shirayama, M., Seth, M., Lee, H.C., Gu, W., Ishidate, T., Conte, D., Jr., and Mello, C.C. (2012).
439 piRNAs initiate an epigenetic memory of nonself RNA in the C. elegans germline. Cell *150*, 65-
440 77.
441 Tang, W., Seth, M., Tu, S., Shen, E.Z., Li, Q., Shirayama, M., Weng, Z., and Mello, C.C. (2018). A
442 Sex Chromosome piRNA Promotes Robust Dosage Compensation and Sex Determination in
443 C. elegans. Dev Cell *44*, 762-770 e763.
444 Updike, D., and Strome, S. (2010). P granule assembly and function in Caenorhabditis elegans
445 germ cells. J Androl *31*, 53-60.
446 Watanabe, T., and Lin, H. (2014). Posttranscriptional regulation of gene expression by Piwi
447 proteins and piRNAs. Mol Cell *56*, 18-27.
448 Weiser, N.E., and Kim, J.K. (2019). Multigenerational Regulation of the Caenorhabditis
449 elegans Chromatin Landscape by Germline Small RNAs. Annu Rev Genet *53*, 289-311.
450 Wolke, U., Jezuit, E.A., and Priess, J.R. (2007). Actin-dependent cytoplasmic streaming in C.
451 elegans oogenesis. Development *134*, 2227-2236.
452

Figure 1

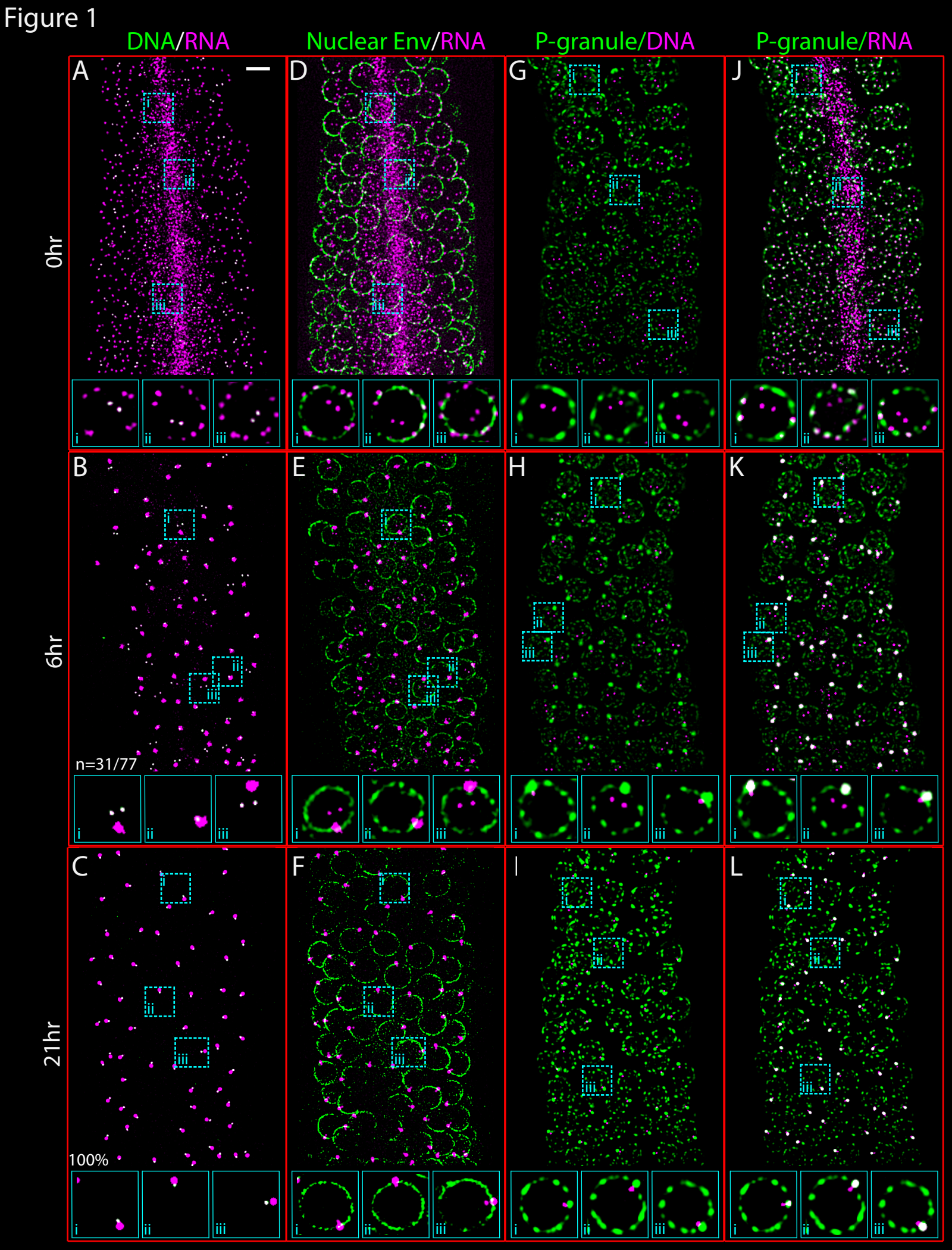
DNA/RNA
Nuclear Env/RNA
P-granule/DNA
P-granule/RNA
0hr
6hr
21hr
A
B
C
D
E
F
G
H
I
J
K
L
n=31/77
100%

Figure 2

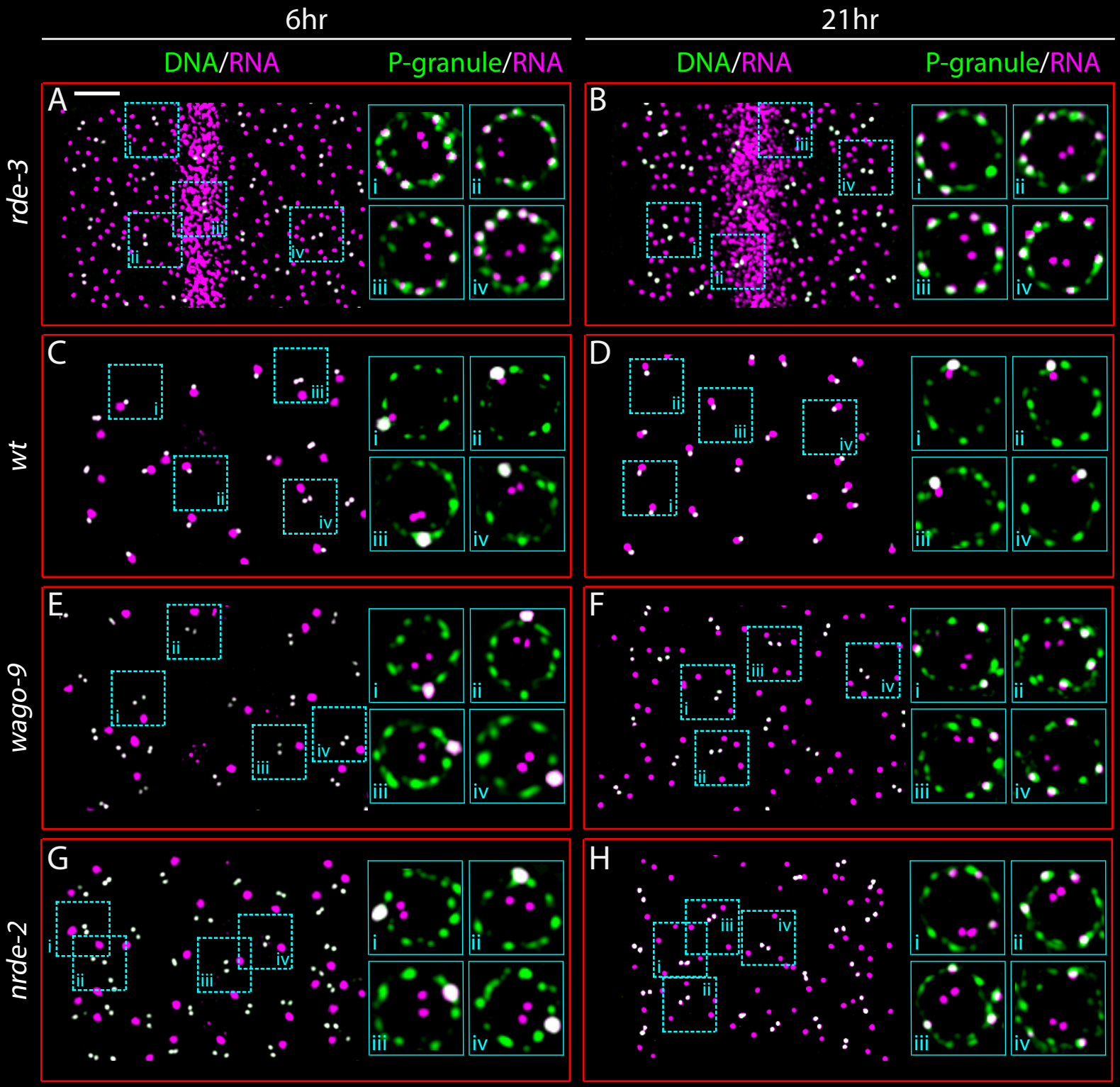
6hr
21hr
DNA/RNA
P-granule/RNA
DNA/RNA
P-granule/RNA
rde-3
wt
wago-9
nrde-2
A
B
C
D
E
F
G
H
i
ii
iii
iv

Figure 3

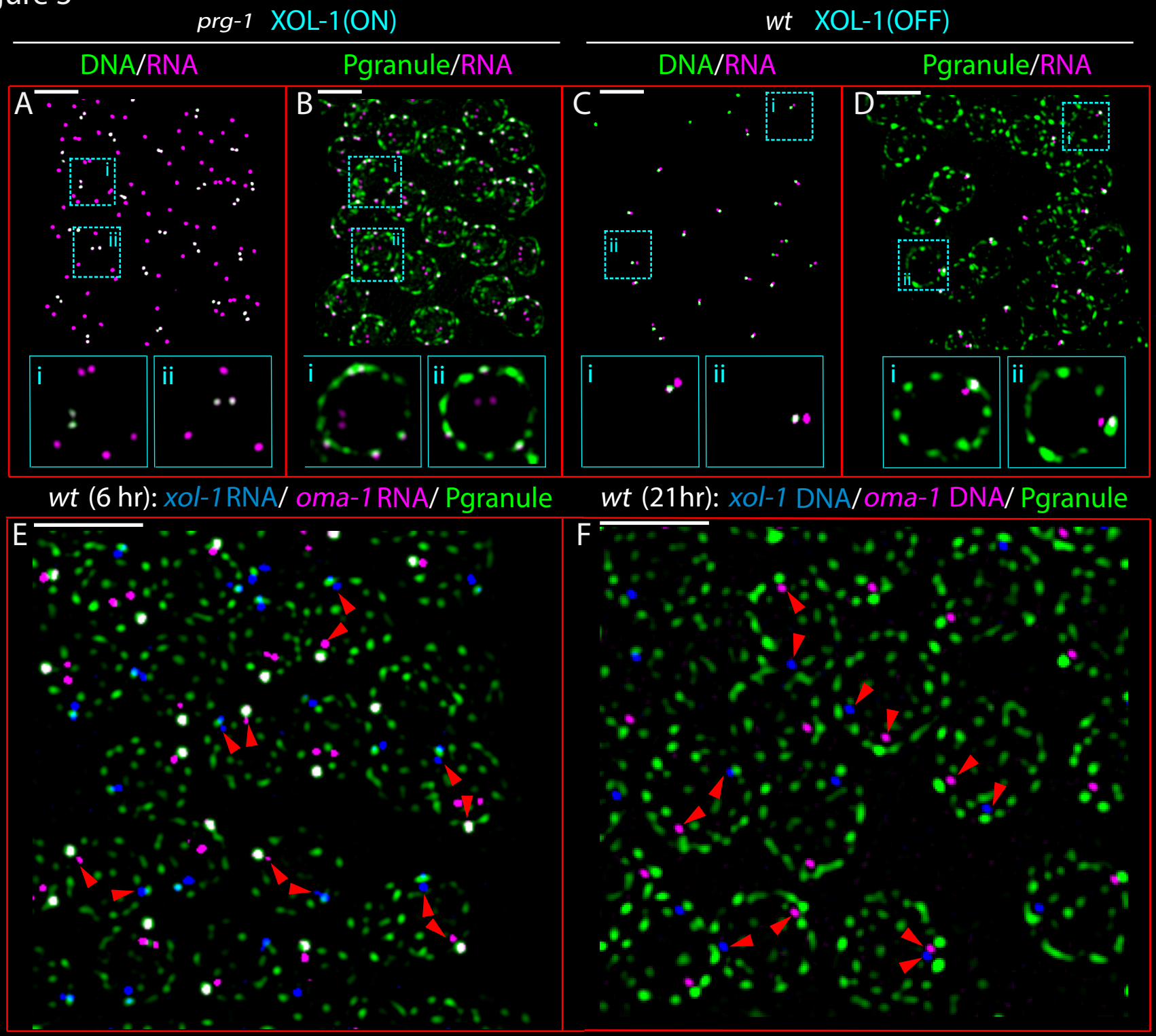
prg-1 XOL-1(ON)
wt XOL-1(OFF)
DNA/RNA
Pgranule/RNA
DNA/RNA
Pgranule/RNA
A
B
C
D
i
ii
wt (6 hr): xol-1 RNA/ oma-1 RNA/ Pgranule
wt (21hr): xol-1 DNA/oma-1 DNA/ Pgranule
E
F

Figure 4 Model

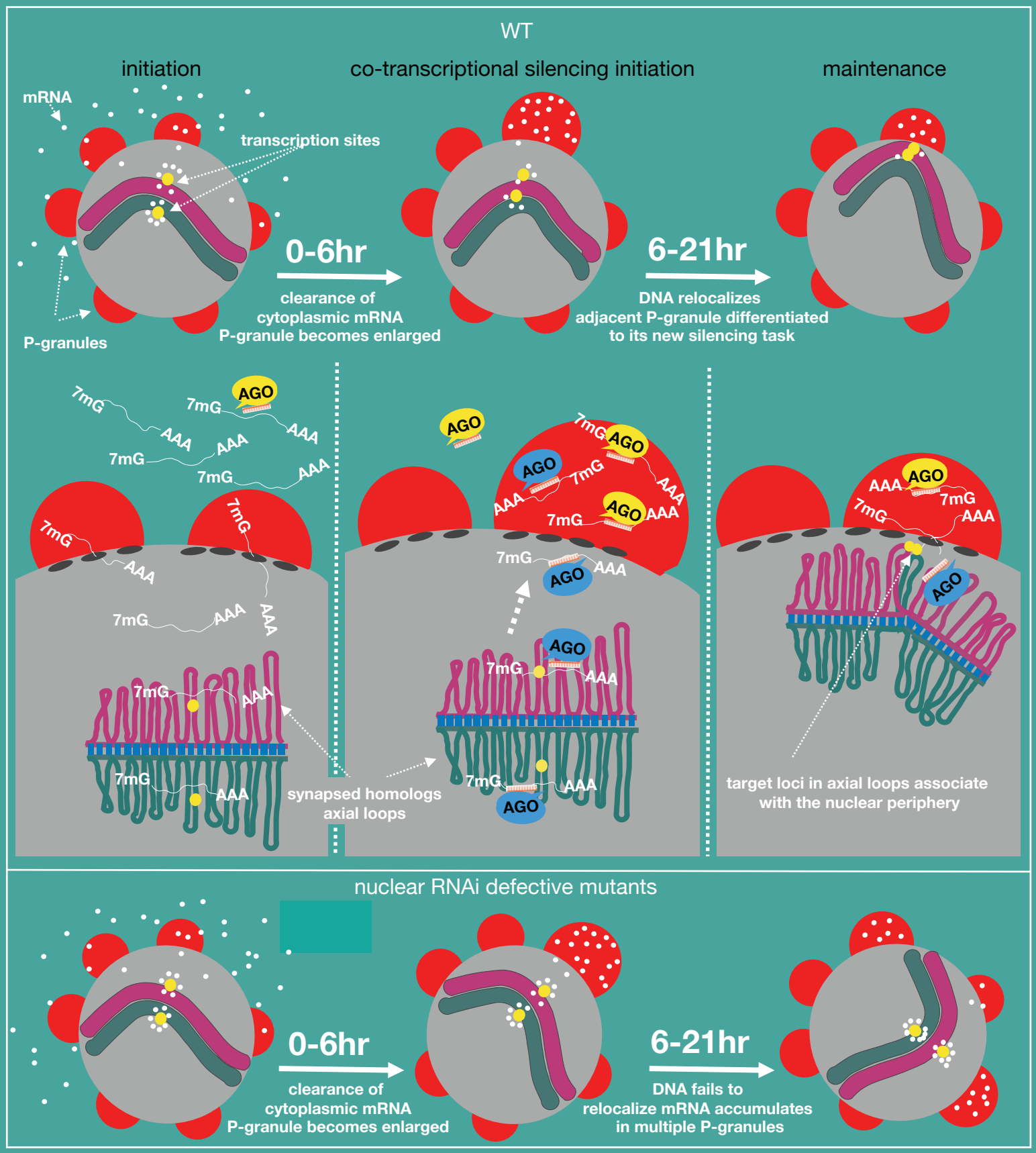
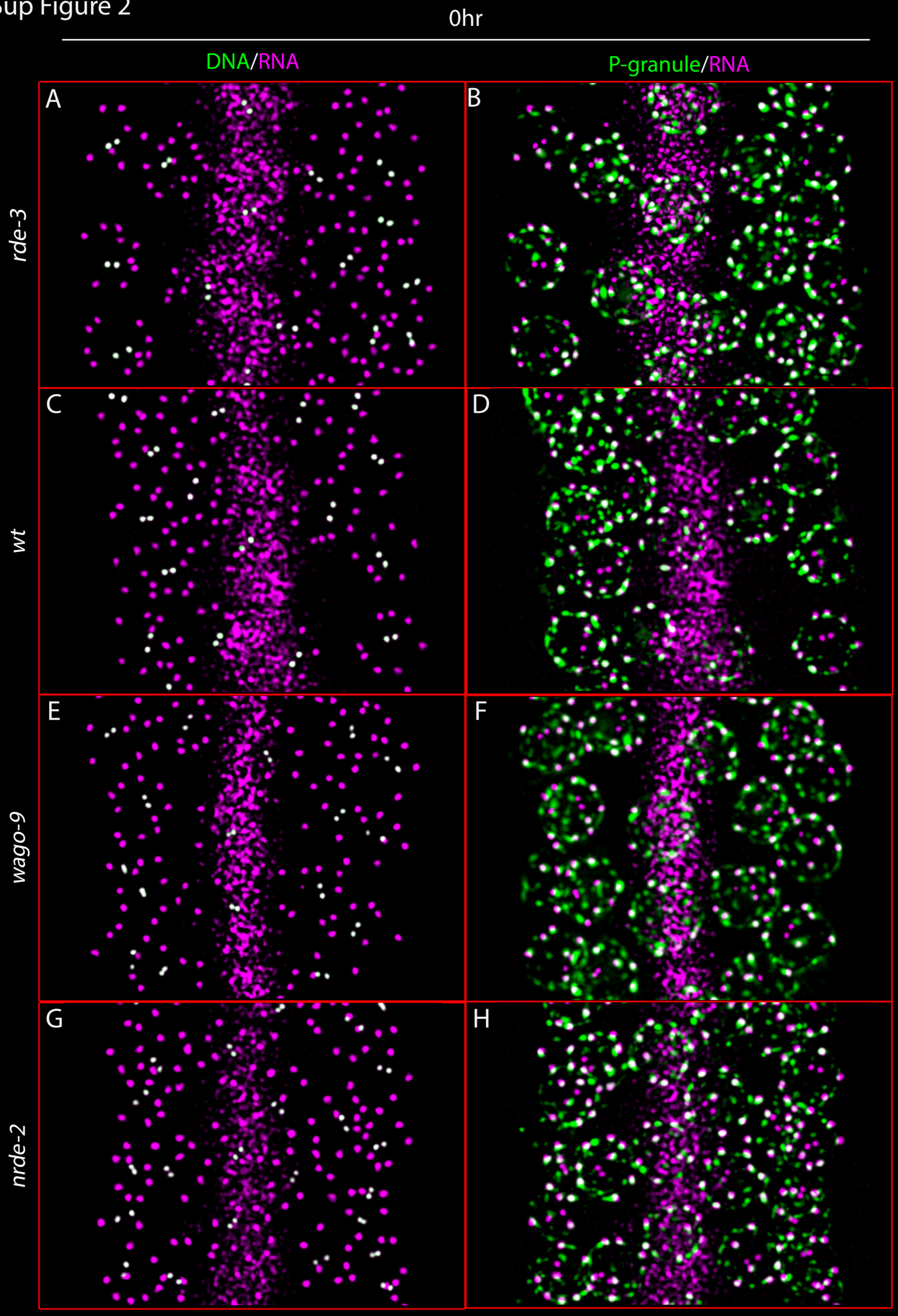
Sup Figure 2